

Article

# Noble Metal Modification of CdS-Covered CuInS<sub>2</sub> Electrodes for Improved Photoelectrochemical Activity and Stability

Toshihiro Takashima <sup>1,2,\*</sup> , Yukitaka Fujishiro <sup>2</sup> and Hiroshi Irie <sup>1,2</sup>

<sup>1</sup> Clean Energy Research Center, University of Yamanashi, 4-3-11 Takeda, Kofu, Yamanashi 400-8511, Japan; hirie@yamanashi.ac.jp

<sup>2</sup> Integrated Graduate School of Medicine, Engineering, and Agricultural Sciences, University of Yamanashi, 4-3-11 Takeda, Kofu, Yamanashi 400-8511, Japan; g19ta038@yamanashi.ac.jp

\* Correspondence: ttakashima@yamanashi.ac.jp

Received: 30 July 2020; Accepted: 18 August 2020; Published: 20 August 2020



**Abstract:** In this paper, efficient and stable photoelectrochemical (PEC) hydrogen (H<sub>2</sub>) evolution using copper indium sulfide (CuInS<sub>2</sub>) thin film electrodes was studied. Modification with a cadmium sulfide (CdS) layer led to improved charge separation at the interface between CuInS<sub>2</sub> and CdS; however, the photocorrosive nature of CdS induced poor stability of the photocathode. Further surface coating with an electrodeposited Pt layer over the CdS-covered CuInS<sub>2</sub> photocathode prevented the CdS layer from making contact with the electrolyte solution, and enabled efficient PEC H<sub>2</sub> evolution without appreciable degradation. This indicates that the Pt layer functioned not only as a reaction site for H<sub>2</sub> evolution, but also as a protection layer. In addition, it was found that surface protection using a noble metal layer was also effective for stable PEC carbon dioxide (CO<sub>2</sub>) reduction when appropriate noble metal cocatalysts were selected. When Au or Ag was used, carbon monoxide was obtained as a product of PEC CO<sub>2</sub> reduction.

**Keywords:** photoelectrochemistry; water splitting; hydrogen; photocathode; carbon dioxide

## 1. Introduction

Hydrogen (H<sub>2</sub>) is a potential clean energy carrier that could replace fossil fuels and solve the associated environmental issues. Photoelectrochemical (PEC) water splitting using sunlight is a promising approach to producing H<sub>2</sub> without emitting carbon dioxide (CO<sub>2</sub>), providing a sustainable future energy supply [1,2]. Since the first demonstration of PEC water splitting using a titanium dioxide (TiO<sub>2</sub>) photoelectrode was reported by Fujishima and Honda [3], semiconductor materials have been extensively studied as photoelectrodes to achieve efficient solar-to-H<sub>2</sub> conversion [4–10].

Copper chalcopyrite compounds, formulated as Cu(In,Ga)(S,Se)<sub>2</sub>, have recently received considerable attention as promising candidates for photocathodes, owing to their high absorption coefficients (>10<sup>4</sup> M<sup>-1</sup> cm<sup>-1</sup>), tunable narrow bandgaps (1.5–2.4 eV), and favorable conduction band positions with respect to the hydrogen evolution reaction (HER) [11–16]. Moreover, the PEC performance of copper chalcopyrite photocathodes has been reported to improve when combined with *n*-type semiconductor buffer layers such as cadmium sulfide (CdS), indium sulfide (In<sub>2</sub>S<sub>3</sub>), and zinc sulfide (ZnS). This is due to the formation of a *p*–*n* junction, which facilitates charge separation at the interface [17–20]. However, to achieve efficient and stable PEC H<sub>2</sub> evolution, further improvements will be necessary to overcome the sluggish surface redox reactions and the instability of sulfide materials in aqueous solutions.

Noble metal cocatalysts such as Pt, Au, and Ag have been widely used to catalyze redox reactions efficiently [21–24]. Their loading not only facilitates the separation of photogenerated charges, but also

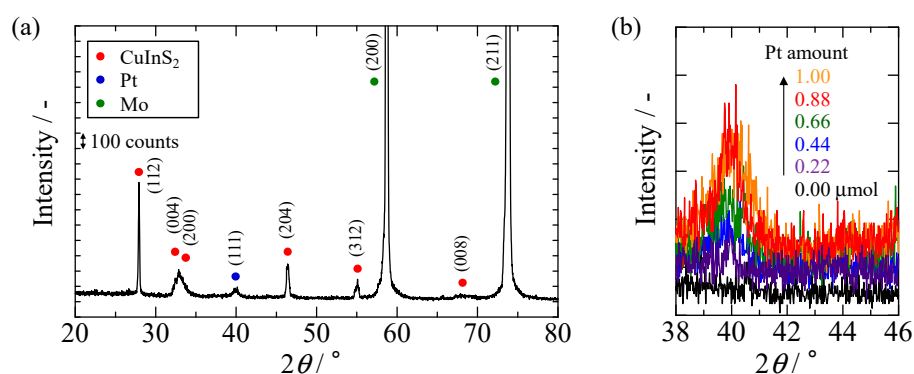
lowers the overpotential for desirable reactions. As such, we considered that using these cocatalysts as coatings could also be effective for improving the stability of photoelectrodes by preventing the exposure of labile electrode surfaces to the electrolyte. For example, Morikawa et al. reported that Rh deposition improved the stability of nitrogen-doped tantalum pentoxide (N-Ta<sub>2</sub>O<sub>5</sub>) photocathodes by suppressing self-reduction of Ta<sup>5+</sup> and/or nitrogen elimination [25]. Li et al. succeeded in almost complete suppression of the degradation of cuprous oxide (Cu<sub>2</sub>O) photocathodes by depositing a thin Ag layer that prevented the self-reduction of Cu<sub>2</sub>O to Cu and the self-oxidation of Cu<sub>2</sub>O to CuO [26]. Nevertheless, there have been few reports on the use of noble metal cocatalysts to suppress the corrosion of metal sulfide photocathodes. Recently, photoelectrodes covered with a metal oxide layers have been developed, and the use of a dense metal oxide layer was demonstrated to be highly effective for improving stability [27–30]. However, the metal oxide protection layer could provide resistance for the extraction of photogenerated charges to the electrode surface, and its preparation required vacuum processes. In contrast, a metal cocatalyst layer would be conductive and could be formed using wet processes. Therefore, the stability improvement provided by metal cocatalyst layer deposition would enable the simple production of active and stable photoelectrodes.

In the present study, we synthesized copper indium sulfide (CuInS<sub>2</sub>) photocathodes modified with CdS and various amounts of electrodeposited Pt. The structural and chemical properties of these electrode surfaces were characterized, and the effect of Pt loading on the H<sub>2</sub>-generation activity and durability in PEC experiments was investigated. Covering the electrode surface with an appropriate amount of Pt cocatalyst enabled persistent PEC H<sub>2</sub> evolution, and it was found that a similar technique was applicable to PEC CO<sub>2</sub> reduction by selecting suitable noble metal cocatalysts. When Au or Ag was loaded on the CdS-modified CuInS<sub>2</sub> electrode, carbon monoxide (CO) production was observed as a result of PEC CO<sub>2</sub> reduction.

## 2. Results and Discussion

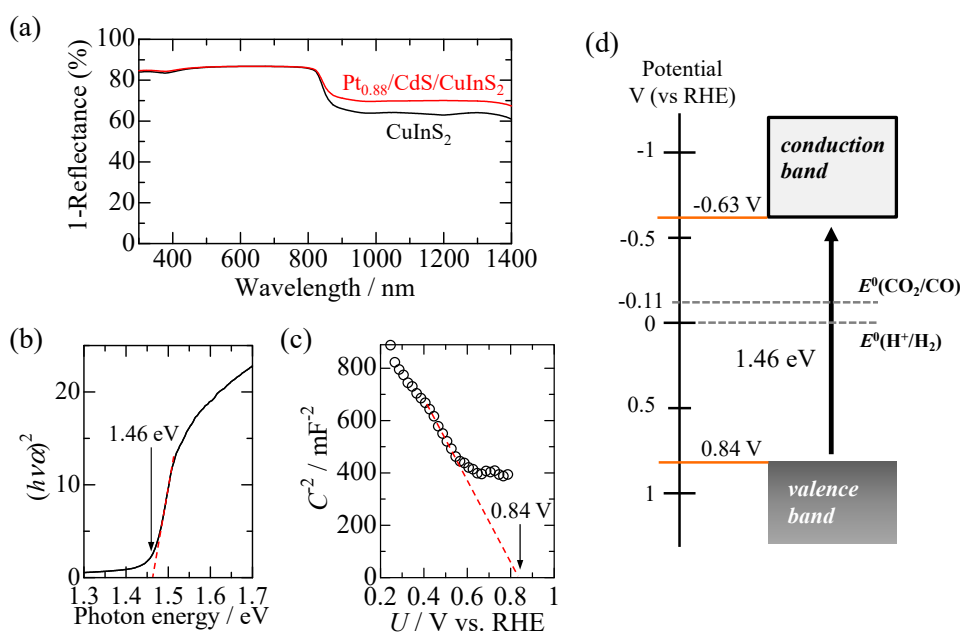
### 2.1. Characterization

The XRD pattern of the electrodeposited Cu/In bilayer film showed diffraction peaks assigned to Cu, In, and CuIn in addition to strong peaks derived from the Mo substrate (Figure S1a). After sulfurization, the electrodeposited metallic precursors were converted to chalcopyrite CuInS<sub>2</sub> without formation of a secondary phase (Figure S1b). Figure 1 shows the XRD pattern of the Pt/CdS/CuInS<sub>2</sub> film, where a peak corresponding to Pt was observed at around 40° in addition to those of CuInS<sub>2</sub> and Mo (the CdS/CuInS<sub>2</sub> electrodes modified with XXX μmol of electrodeposited Pt are denoted as Pt<sub>xxx</sub>/CdS/CuInS<sub>2</sub>). No peak assigned to CdS was observed, as the layer was too thin.



**Figure 1.** (a) XRD pattern of Pt<sub>0.88</sub>/CdS/CuInS<sub>2</sub> electrode. Red, blue, and green dots indicate the positions of the peaks in the standard patterns of CuInS<sub>2</sub> (ICDD #01-082-1702), Pt (ICDD #03-065-7442), and Mo (ICDD #01-087-0646), respectively. (b) Magnified patterns around the Pt peak for Pt/CdS/CuInS<sub>2</sub> electrodes.

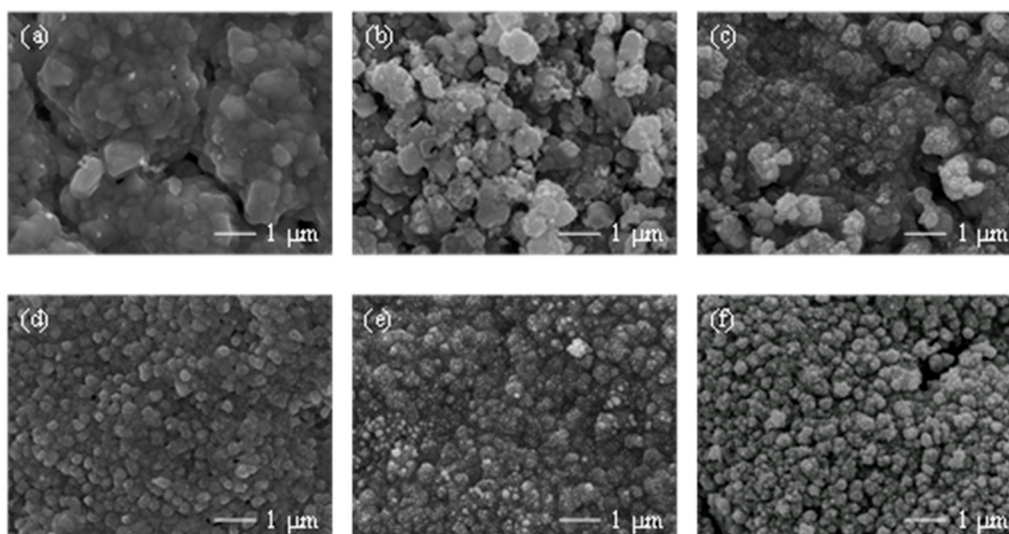
Figure 2a shows UV-vis-NIR absorption spectra of the CuInS<sub>2</sub> and Pt<sub>0.88</sub>/CdS/CuInS<sub>2</sub> films. As reported in the literature, the CuInS<sub>2</sub> film showed intense absorption over a wide wavelength range from 300 to 850 nm [14,31,32]. The bandgap was calculated to be 1.46 eV using a Tauc plot (Figure 2b), and the flat band potential was determined to be approximately 0.84 V using a Mott–Schottky plot (Figure 2c), indicating that the band position of the prepared CuInS<sub>2</sub> film (Figure 2d) was in accordance with that previously determined by photoelectron spectroscopy [13,18]. The Pt<sub>0.88</sub>/CdS/CuInS<sub>2</sub> film showed an absorption spectrum similar to that of the CuInS<sub>2</sub> film, with an increase in absorption being observed at wavelengths above 820 nm (Figure 2a). The origin of this increased absorption is considered to be light scattering by the deposited Pt, which has often been observed for photocatalysts modified with Pt nanoparticles [33,34].



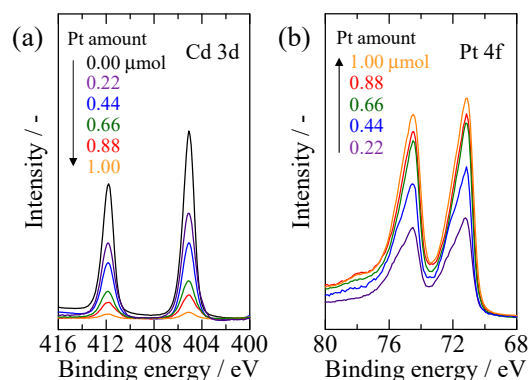
**Figure 2.** (a) UV-vis-NIR absorption spectra of CuInS<sub>2</sub> and Pt<sub>0.88</sub>/CdS/CuInS<sub>2</sub> electrodes. (b) Tauc plot and (c) Mott–Schottky plot of CuInS<sub>2</sub> electrode. (d) Band alignment of the synthesized CuInS<sub>2</sub> electrode deduced from the results shown in (a–c).

The morphological features of the synthesized films were investigated by SEM. Top-down and cross-sectional views of the CuInS<sub>2</sub> film (Figure S2) revealed that it consisted of a dense crystalline layer accompanied by plate-like particles on the surface, and its thickness was found to be about 1.3  $\mu\text{m}$ . After modification with CdS, the surface became relatively smooth and porous (Figure 3a). In contrast, the formation of nanoparticles, with diameter of approximately 10 nm, was observed for the Pt-deposited samples (Figure S3), and higher amounts of Pt deposition resulted in a more granular surface (Figure 3b–f). Furthermore, it was observed that Pt particles not only formed on the CdS grains, but also filled the pores of the CdS, suggesting that the CdS surface was entirely covered when depositing a sufficient amount of Pt.

This suggestion was supported by the XPS results. Figure 4a,b shows the XPS spectra of CdS/CuInS<sub>2</sub> and Pt/CdS/CuInS<sub>2</sub> films for the Cd 3d (Figure 4a) and Pt 4f (Figure 4b) regions, respectively. As Pt loading was increased, the Cd 3d peaks significantly weakened while the Pt 4f peaks became stronger, with the Cd 3d peaks almost disappearing in the case of Pt<sub>100</sub>/CdS/CuInS<sub>2</sub>. On the basis of these results, it was anticipated that the CdS layer could be protected during PEC H<sub>2</sub> evolution by depositing Pt onto the surface.



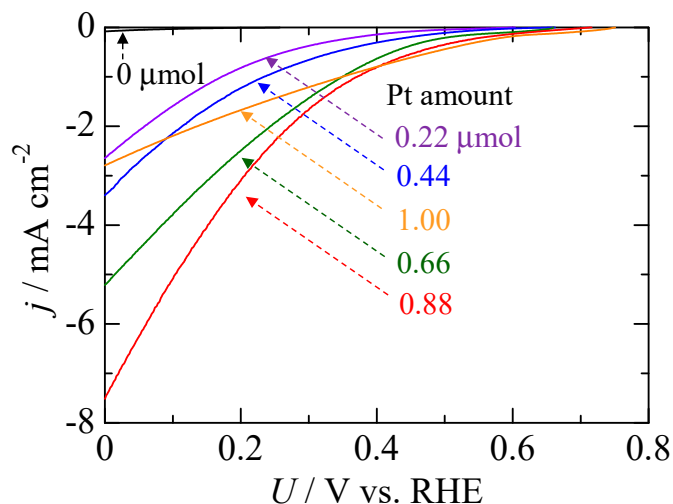
**Figure 3.** SEM images of (a) CdS/CuInS<sub>2</sub>, (b) Pt<sub>0.22</sub>/CdS/CuInS<sub>2</sub>, (c) Pt<sub>0.44</sub>/CdS/CuInS<sub>2</sub>, (d) Pt<sub>0.66</sub>/CdS/CuInS<sub>2</sub>, (e) Pt<sub>0.88</sub>/CdS/CuInS<sub>2</sub>, and (f) Pt<sub>1.00</sub>/CdS/CuInS<sub>2</sub>.



**Figure 4.** XPS spectra in the (a) Cd 3d and (b) Pt 4f regions of Pt/CdS/CuInS<sub>2</sub> with various Pt loadings.

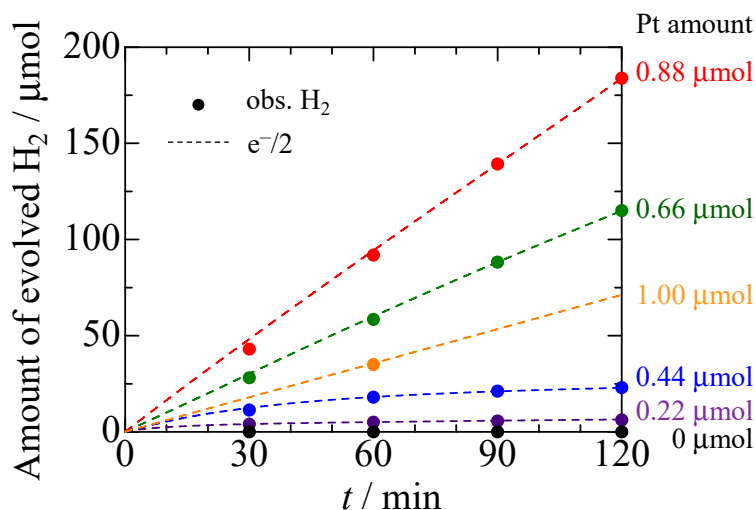
## 2.2. Photoelectrochemical Measurements

The PEC properties of the prepared electrodes were examined by linear sweep voltammetry measured under visible light irradiation. Although the bare CuInS<sub>2</sub> electrode showed limited photoresponse (Figure S4), a distinct cathodic photocurrent was generated after modification with both CdS and Pt. This is because the CdS layer deposited on CuInS<sub>2</sub> possessed suitable band characteristics for the formation of a *p-n* junction (Figure 2d and Figure S5), facilitating extraction of excited electrons from the inside of CuInS<sub>2</sub> to the electrode surface, while Pt acted as a cocatalyst to reduce overpotential for H<sub>2</sub> evolution. Consequently, modification with these materials enabled the extraction of photoexcited electrons from CuInS<sub>2</sub> to the electrolyte. In contrast, the modification with only CdS made no increase in photocurrent (Figure S4). Figure 5 shows polarization curves of the Pt-modified CdS/CuInS<sub>2</sub> electrodes with different Pt contents. As the amount of Pt was increased up to 0.88 μmol, a gradual improvement in photocurrent density and a positive shift in the onset potential were observed; in contrast, the increase in Pt loading had almost no effect on current generation under dark conditions (Figure S6). However, further increases in Pt content above 0.88 μmol were detrimental to current density, as excess Pt loading limited light absorption by CuInS<sub>2</sub>. Thus, the largest photoresponse was observed for Pt<sub>0.88</sub>/CdS/CuInS<sub>2</sub>, with its photocurrent reaching 7.5 mA cm<sup>-2</sup> at 0 V. This value is about half of the photocurrent recorded using the Pt/CdS/(CuInS<sub>2</sub>)<sub>0.81</sub> (ZnS)<sub>0.19</sub> electrode which is a state-of-the-art CuInS<sub>2</sub>-based photocathode prepared by tuning the band position of the light absorber [12].



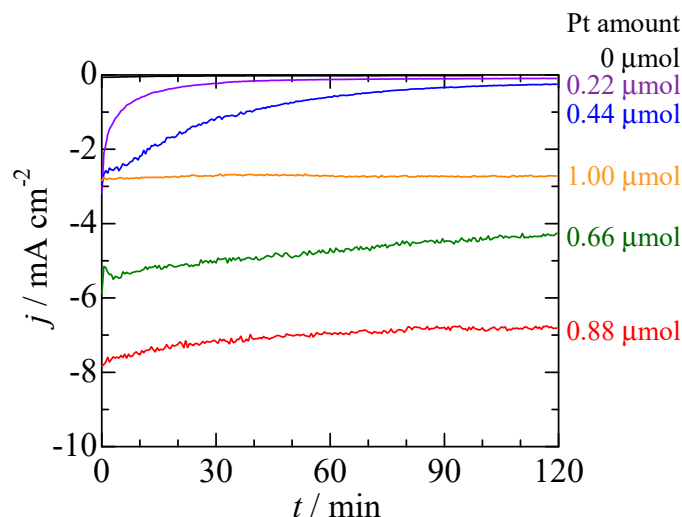
**Figure 5.** Polarization curves of Pt/CdS/CuInS<sub>2</sub> photoelectrodes measured under visible light irradiation ( $\lambda > 420$  nm).

To confirm the H<sub>2</sub> generation ability of the Pt/CdS/CuInS<sub>2</sub> electrode, the amount of H<sub>2</sub> evolved during photoelectrolysis was quantified. Figure 6 shows the typical time courses of H<sub>2</sub> evolution over the Pt/CdS/CuInS<sub>2</sub> photoelectrodes with an applied potential of 0 V and one-half of the electrons passing through the outer circuit ( $e^-/2$ ). Continuous H<sub>2</sub> production was observed for all the photoelectrodes, and approximately 180  $\mu\text{mol}$  of H<sub>2</sub> generated over Pt<sub>0.88</sub>/CdS/CuInS<sub>2</sub> after illumination for 120 min. The faradaic efficiency, defined as the ratio of the amount of H<sub>2</sub> to that of  $e^-/2$ , was calculated to be over 99% for all the Pt/CdS/CuInS<sub>2</sub> photoelectrodes, indicating that no reduction reactions other than H<sub>2</sub> evolution proceeded, irrespective of the amount of Pt.



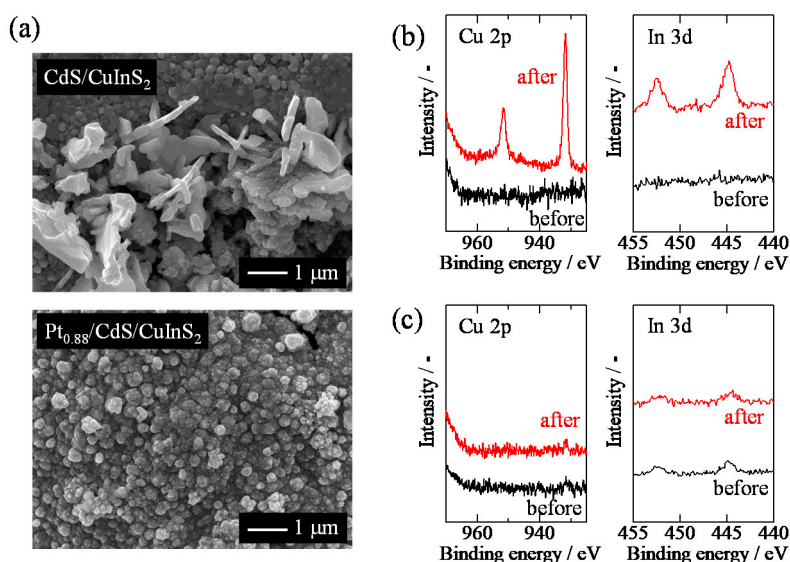
**Figure 6.** Time course curves of H<sub>2</sub> evolution (closed circles) from Pt/CdS/CuInS<sub>2</sub> electrodes measured at 0 V under irradiation with visible light ( $\lambda > 420$  nm). The broken lines denote time course curves of half of the electrons passing through the outer circuit ( $e^-/2$ ).

Figure 7 shows typical photocurrent time profiles measured during PEC H<sub>2</sub> evolution experiments. These results indicate that the stability of the Pt/CdS/CuInS<sub>2</sub> photoelectrodes significantly depended on the Pt loading. Although rapid photocurrent decays were observed for Pt<sub>0.22</sub>/CdS/CuInS<sub>2</sub> and Pt<sub>0.44</sub>/CdS/CuInS<sub>2</sub>, a significant improvement in the stability was observed at higher Pt loadings, with Pt<sub>100</sub>/CdS/CuInS<sub>2</sub> retaining 99% of its photocurrent after photoelectrolysis. Photocurrent decay in CdS-modified photocathodes has previously been studied by several groups, and the phenomenon was attributed to the poor stability of CdS due to photocorrosion [28,35].



**Figure 7.** Current–time profiles of Pt/CdS/CuInS<sub>2</sub> electrodes measured at 0 V under irradiation with visible light ( $\lambda > 420$  nm).

Figure 8a shows SEM images of CdS/CuInS<sub>2</sub> and Pt<sub>0.88</sub>/CdS/CuInS<sub>2</sub> photoelectrodes after stability tests. In the image of CdS/CuInS<sub>2</sub>, the disappearance of CdS and exposure of plate-like CuInS<sub>2</sub> particles were observed in some areas, whereas the Pt<sub>0.88</sub>/CdS/CuInS<sub>2</sub> electrode showed few changes other than the aggregation of Pt particles. The XPS spectra also showed evidence of the photocorrosion of CdS for the CdS/CuInS<sub>2</sub> electrode, with an increase in the Cu 2p and In 3d peaks being observed after photoelectrolysis (Figure 8b). In contrast, the Cu 2p and In 3d spectra of the Pt<sub>0.88</sub>/CdS/CuInS<sub>2</sub> electrode remained unchanged (Figure 8c). Therefore, Pt modification was found to be effective for both promoting PEC H<sub>2</sub> evolution and improving the stability of the CdS/CuInS<sub>2</sub> photocathode.



**Figure 8.** (a) SEM images of CdS/CuInS<sub>2</sub> (upper) and Pt<sub>0.88</sub>/CdS/CuInS<sub>2</sub> (lower) photoelectrodes after 120 min of photoelectrolysis. (The SEM images of CdS/CuInS<sub>2</sub> and Pt<sub>0.88</sub>/CdS/CuInS<sub>2</sub> photoelectrodes before the photoelectrolysis are shown in Figure 3a,e, respectively.) Comparison of XPS spectra of (b) CdS/CuInS<sub>2</sub> and (c) Pt<sub>0.88</sub>/CdS/CuInS<sub>2</sub> electrodes before and after 120 min of photoelectrolysis.

### 2.3. Photoelectrochemical CO<sub>2</sub> Reduction

Finally, we examined PEC CO<sub>2</sub> reduction using noble-metal-modified CuInS<sub>2</sub> electrodes in CO<sub>2</sub>-saturated NaHCO<sub>3</sub> solutions. As was the case for PEC H<sub>2</sub> generation, the photoresponse of the

bare CuInS<sub>2</sub> film was so small that CdS and metal cocatalysts were deposited to enhance photoreactivity. For this experiment, Au and Ag were used as cocatalysts in addition to Pt because electrochemical CO<sub>2</sub> reduction using Au and Ag has shown high activity and selectivity for CO formation [36,37]. The loadings of all the cocatalysts were adjusted to 0.88 μmol based on the PEC H<sub>2</sub> generation results achieved using the Pt/CdS/CuInS<sub>2</sub> photocathode. Table 1 shows the results of PEC CO<sub>2</sub> reduction conducted at −0.11 V under visible light irradiation. By adding metal cocatalysts, the photocurrent density increased in the order of Pt > Au > Ag; however, the photocurrent of Pt<sub>0.88</sub>/CdS/CuInS<sub>2</sub> was much smaller than that measured for PEC H<sub>2</sub> evolution. It is notable that deactivation during PEC CO<sub>2</sub> reduction can occur not only due to corrosion of CdS but also due to the poisoning of the cocatalyst. This photocurrent decrease was presumed to be caused by the poisoning of the Pt cocatalyst because CO molecules formed as the intermediate species occupied the active sites of Pt without being released into the solution [38]. In fact, product analysis indicated that a negligible amount of CO<sub>2</sub> reduction products was formed and that the faradaic efficiency for H<sub>2</sub> evolution was almost 100%, although CO<sub>2</sub> reduction by photoexcited electrons generated in Pt<sub>0.88</sub>/CdS/CuInS<sub>2</sub> was thermodynamically favorable. Furthermore, XPS spectra measured after photoelectrolysis showed no increase in the peaks assigned to Cu and In, suggesting that CdS photocorrosion was also suppressed in this experiment (Figure S7). When Au/CdS/CuInS<sub>2</sub> and Ag/CdS/CuInS<sub>2</sub> were employed for PEC CO<sub>2</sub> reduction, continuous CO production was observed, with the faradaic efficiencies for CO formation over Au/CdS/CuInS<sub>2</sub> and Ag/CdS/CuInS<sub>2</sub> being 6.7% and 3.5%, respectively. Although most of the photocurrent was still derived from H<sub>2</sub> evolution, the observed faradaic efficiencies for CO formation were relatively high compared to other relevant studies reported so far [39–41]. In addition, the CO<sub>2</sub> reduction photocurrent density (ca. 100 μA/cm<sup>2</sup>) observed using Au/CdS/CuInS<sub>2</sub> was about 80-fold higher than that observed for CuGaS<sub>2</sub>, which is the only copper chalcopyrite compound reported for PEC CO<sub>2</sub> reduction [40].

**Table 1.** Photoelectrochemical CO<sub>2</sub> reduction using CdS/CuInS<sub>2</sub> electrodes modified with noble metal cocatalysts.

Photoelectrode	<i>j</i> (mA/cm <sup>2</sup> at −0.11 V)	Faradaic Efficiency (%)	
		H <sub>2</sub>	CO
Pt <sub>0.88</sub> /CdS/CuInS <sub>2</sub>	4.0	99	0.36
Au/CdS/CuInS <sub>2</sub>	1.5	93	6.7
Ag/CdS/CuInS <sub>2</sub>	0.21	69	3.5

SEM observation showed that both the Au and Ag cocatalysts had dendritic structures (Figure S8), and similar-shaped electrocatalysts have been reported to convert CO<sub>2</sub> to CO with high selectivities of over 80% when overpotentials of 0.3–0.5 V are applied [42,43]. According to the conduction band minimum (CBM) potential of CdS [14,17], photoexcited electrons in the Au/CdS/CuInS<sub>2</sub> and Ag/CdS/CuInS<sub>2</sub> photocathodes were considered to possess reduction potentials of around −0.3 V, corresponding to 0.19 V of overpotentials. Recently, the CBM potential of CdS was found to be tunable by forming a solid solution with ZnS, and the introduction of ZnS shifted the CBM to a more negative potential [44]. Furthermore, a thin film of CdS–ZnS solid solution can be formed by the chemical bath deposition (CBD) method [45], which was used for deposition of the CdS layer in this study. Thus, the utilization of a CdS–ZnS solid solution layers in combination with appropriate amounts of Au and Ag cocatalysts would offer the possibility to achieve PEC CO<sub>2</sub> reduction with high selectivity and durability, and such studies are underway in our laboratory.

### 3. Materials and Methods

#### 3.1. Chemicals

Copper sulfate (CuSO<sub>4</sub>), indium chloride (InCl<sub>3</sub>), citric acid, trisodium citrate, sulfur, potassium cyanide (KCN), cadmium sulfate (CdSO<sub>4</sub>), thiourea, hydrogen hexachloroplatinate (H<sub>2</sub>PtCl<sub>6</sub>),

hydrochloric acid (HCl), ammonium hydroxide (NH<sub>4</sub>OH), sodium sulfate (Na<sub>2</sub>SO<sub>4</sub>), potassium dihydrogen phosphate (KH<sub>2</sub>PO<sub>4</sub>), and sodium bicarbonate (NaHCO<sub>3</sub>) were obtained from Kanto Chemical Co., Inc. (Japan). All chemicals were used without further purification.

### 3.2. Preparation of CuInS<sub>2</sub> Film on Mo Foil

CuInS<sub>2</sub> thin film electrodes were synthesized using electrodeposition and subsequent sulfurization, as reported in the literature [14,31,32]. Prior to electrodeposition, Mo foil (Nilaco, Japan, 99.95%, 0.15 mm thickness) was cleaned by sonicating for 30 min in 0.1 M HCl. Electrodeposition was conducted using an electrochemical analyzer (HZ-5000, Hokuto Denko, Japan) and a single cell with a three-electrode setup consisting of the Mo foil, a Pt wire, and a silver/silver chloride (Ag/AgCl) electrode, which functioned as the working, counter, and reference electrodes, respectively. Metallic Cu and In layers were successively deposited onto the Mo foil under potentiostatic conditions. Cu deposition was conducted at  $-0.2$  V vs. Ag/AgCl in an aqueous solution containing 50 mM CuSO<sub>4</sub>, 242 mM citric acid, and 150 mM trisodium citrate. Subsequently, In deposition onto the Cu layer was performed at  $-0.76$  V vs. Ag/AgCl in an aqueous solution containing 30 mM InCl<sub>3</sub>·4H<sub>2</sub>O, 36 mM citric acid, and 242 mM trisodium citrate. The amount of deposited Cu and In was controlled by adjusting the electric charge to 1042 and 1200 mC/cm<sup>2</sup>, respectively. The as-prepared Cu/In film was sealed in an evacuated Pyrex ampule with 5 mg of elemental sulfur and then sulfurized by heating at 600 °C for 10 min. Finally, the thus-obtained CuInS<sub>2</sub> films were etched by immersion in an aqueous KCN solution (10%) for 2 min to remove excess Cu<sub>x</sub>S.

### 3.3. Surface Modification of CuInS<sub>2</sub> Electrode

The CuInS<sub>2</sub> electrode was modified with CdS by the CBD method. The CuInS<sub>2</sub> electrode was immersed in an aqueous solution containing 12.5 mM CdSO<sub>4</sub>, 0.22 M thiourea, and 11 M NH<sub>4</sub>OH for 7 min at 60 °C. After the modification, the electrode was thoroughly rinsed with distilled water and dried at room temperature. CuInS<sub>2</sub> electrodes modified with CdS are hereafter denoted as CdS/CuInS<sub>2</sub>. The Pt cocatalyst was deposited on the CdS/CuInS<sub>2</sub> electrode by photoelectrodeposition. The electrode was immersed in 0.1 M Na<sub>2</sub>SO<sub>4</sub> solution (pH 4.0) containing 1 mM H<sub>2</sub>PtCl<sub>6</sub>, and the electrodeposition was carried out at  $-0.1$  V vs. Ag/AgCl under illumination with a Xe lamp (LA-251 Xe; Hayashi Tokei). The amount of Pt was controlled to 0.22, 0.44, 0.66, 0.88, and 1.00 μmol by monitoring the electric charge passed through the electrode, and the electrode was then thoroughly rinsed with distilled water and dried at room temperature. Thus, the photoelectrode was prepared and its surface area was set to 0.7 cm<sup>2</sup> (0.7 cm × 1.0 cm). Hereafter, the electrodes thus obtained are denoted as Pt<sub>xxx</sub>/CdS/CuInS<sub>2</sub>, where XXX corresponds to the amount of electrodeposited Pt. HAuCl<sub>4</sub> (6 mM) and AgNO<sub>3</sub> (5 mM) were used as the electrolytes for the preparation of the Au- and Ag-deposited samples, respectively, with these being denoted as Au/CdS/CuInS<sub>2</sub> and Ag/CdS/CuInS<sub>2</sub>, respectively.

### 3.4. Characterization

XRD patterns were obtained using a PW-1700 system (PANalytical, Almelo, The Netherlands). The morphologies of the prepared films were observed by SEM (JSM-6500F, JEOL, Tokyo, Japan). Optical absorption spectra were measured in diffuse reflectance (DR) mode using a UV-vis-NIR spectrometer (UV-2600, Shimadzu, Kyoto, Japan) with barium sulfate (BaSO<sub>4</sub>) as the reflectance standard. XPS were measured using an X-ray photoelectron spectrometer (AXIS-ULTRA, KRATOS, Stretford, UK). The C 1s peak (284.6 eV) was used as an internal energy reference in all the experiments. Mott–Schottky plots were recorded using an electrochemical analyzer equipped with a frequency response analyzer. The electrode potential was scanned at a frequency of 10 Hz in a 1 M Na<sub>2</sub>SO<sub>4</sub> aqueous solution (pH 6.0) that was purged with Ar prior to each experiment.

### 3.5. Photoelectrochemical Measurements

PEC measurements were performed using the same three-electrode setup as used for the preparation of the CuInS<sub>2</sub> electrodes. The electrolyte solutions used for H<sub>2</sub> evolution and CO<sub>2</sub> reduction were Ar-saturated 0.2 M KH<sub>2</sub>PO<sub>4</sub> (pH 6.0) and CO<sub>2</sub>-saturated 0.5 M NaHCO<sub>3</sub> (pH 6.8), respectively. Prior to the measurements, Ar or CO<sub>2</sub> gas was purged through the electrolyte for 20 min to remove dissolved oxygen. A Xe lamp with an optical filter (>420 nm, Y-44, Hoya) was used as a light source. All measured potentials were converted to the reversible hydrogen electrode (RHE) scale using the following equation:  $E_{\text{RHE}} = E_{\text{Ag/AgCl}} + 0.059 \times \text{pH} + 0.199$ .

During the measurements, Ar or CO<sub>2</sub> gas was purged through the electrolyte at a flow rate of 20 mL min<sup>-1</sup> and collected in a clean plastic bag (Smart Bag PA, GL Sciences) along with gaseous products. Evolved H<sub>2</sub> was quantified using a gas chromatograph (GC-8A, Shimadzu) equipped with a thermal conductivity detector (TCD). For the quantification of CO, a gas chromatograph (GC-8A, Shimadzu) equipped with a methanizer and a flame ionization detector (FID) was used.

## 4. Conclusions

In this study, we investigated the effect of Pt loading on the PEC H<sub>2</sub>-evolution activity and durability of CdS/CuInS<sub>2</sub> photocathodes. Structural and chemical characterization of the surface revealed that electrodeposited Pt covered the CdS surface, and the porous structure was filled with Pt by increasing the loading amount. This prevented the exposure of the CdS layer to the electrolyte. PEC experiments showed that the H<sub>2</sub>-evolution activity could be enhanced by Pt modification, resulting in both an increase in photocurrent density and a positive shift in the onset potential. As a result, efficient PEC H<sub>2</sub> evolution proceeded over the Pt/CdS/CuInS<sub>2</sub> photocathodes without appreciable degradation. In addition, the suppression of CdS corrosion using noble metals was also effective for PEC CO<sub>2</sub> reduction experiments, and CO generation was observed when Au or Ag was electrodeposited instead of Pt.

**Supplementary Materials:** The following are available online at <http://www.mdpi.com/2073-4344/10/9/949/s1>, Figure S1: XRD patterns of CuInS<sub>2</sub> electrode measured before and after sulfurization, Figure S2: Top-down and cross-sectional views of CuInS<sub>2</sub> film, Figure S3: Magnified SEM image of Pt<sub>0.88</sub>/CdS/CuInS<sub>2</sub> electrode, Figure S4: Polarization curves of CuInS<sub>2</sub>, CdS/CuInS<sub>2</sub>, and Pt<sub>0.88</sub>/CdS/CuInS<sub>2</sub> electrodes measured under irradiation of visible light, Figure S5: Band characteristics of the prepared CdS film, Figure S6: Polarization curves of CdS/CuInS<sub>2</sub> electrodes modified with various amount of Pt, Figure S7: XPS spectra of Pt<sub>0.88</sub>/CdS/CuInS<sub>2</sub> electrode measured before and after photoelectrochemical CO<sub>2</sub> reduction experiment, Figure S8: SEM images of Au/CdS/CuInS<sub>2</sub> and Ag/CdS/CuInS<sub>2</sub> electrodes.

**Author Contributions:** Conceptualization, T.T.; methodology, T.T. and Y.F.; validation, T.T. and Y.F.; formal analysis, T.T. and Y.F.; investigation, Y.F.; writing—original draft preparation, T.T.; writing—review and editing, T.T. and H.I.; supervision, H.I.; project administration, T.T. and H.I. All authors have read and agreed to the published version of the manuscript.

**Funding:** This research was funded by JSPS KAKENHI Grant-in-Aid for Early-Career Scientists (Grant#18K14315) and by JKA and its promotion funds from KEIRIN RACE (2018M-176).

**Conflicts of Interest:** The authors declare no conflict of interest.

## References

1. Sivula, K.; van de Krol, R. Semiconducting Materials for Photoelectrochemical Energy Conversion. *Nat. Rev. Mater.* **2016**, *1*, 15010. [[CrossRef](#)]
2. Tilley, S.D. Recent Advances and Emerging Trends in Photo-Electrochemical Solar Energy Conversion. *Adv. Energy Mater.* **2019**, *9*, 1802877. [[CrossRef](#)]
3. Fujishima, A.; Honda, K. Electrochemical Photolysis of Water at a Semiconductor Electrode. *Nature* **1972**, *238*, 37–38. [[CrossRef](#)] [[PubMed](#)]
4. Luo, Z.; Wang, T.; Gong, J. Single-Crystal Silicon-Based Electrodes for Unbiased Solar Water Splitting: Current Status and Prospects. *Chem. Soc. Rev.* **2019**, *48*, 2158–2181. [[CrossRef](#)]

5. Varadhan, P.; Fu, H.C.; Kao, Y.C.; Horng, R.H.; He, J.H. An Efficient and Stable Photoelectrochemical System with 9% Solar-to-Hydrogen Conversion Efficiency via InGaP/GaAs Double Junction. *Nat. Commun.* **2019**, *10*, 5282. [[CrossRef](#)]
6. Yang, Y.; Niu, S.; Han, D.; Liu, T.; Wang, G.; Li, Y. Progress in Developing Metal Oxide Nanomaterials for Photoelectrochemical Water Splitting. *Adv. Energy Mater.* **2017**, *7*, 1700555. [[CrossRef](#)]
7. Lee, D.K.; Lee, D.; Lumley, M.A.; Choi, K.S. Progress on Ternary Oxide-Based Photoanodes for Use in Photoelectrochemical Cells for Solar Water Splitting. *Chem. Soc. Rev.* **2019**, *48*, 2126–2157. [[CrossRef](#)]
8. Faraji, M.; Yousefi, M.; Yousefzadeh, S.; Zirak, M.; Naseri, N.; Jeon, T.H.; Choi, W.; Moshfegh, A.Z. Two-Dimensional Materials in Semiconductor Photoelectrocatalytic Systems for Water Splitting. *Energy Environ. Sci.* **2019**, *12*, 59–95. [[CrossRef](#)]
9. Jang, Y.J.; Lee, J.S. Photoelectrochemical Water Splitting with *p*-Type Metal Oxide Semiconductor Photocathodes. *ChemSusChem* **2018**, *12*, 1835–1845. [[CrossRef](#)]
10. Yang, W.; Moon, J. Recent Advances in Earth-Abundant Photocathodes for Photoelectrochemical Water Splitting. *ChemSusChem* **2018**, *12*, 1889–1899. [[CrossRef](#)]
11. Ikeda, S.; Nakamura, T.; Lee, S.M.; Yagi, T.; Harada, T.; Minegishi, T.; Matsumura, M. Photoreduction of Water by Using Modified CuInS<sub>2</sub> Electrodes. *ChemSusChem* **2010**, *4*, 262–268. [[CrossRef](#)] [[PubMed](#)]
12. Zhao, J.; Minegishi, T.; Kaneko, H.; Ma, G.; Zhong, M.; Nakabayashi, M.; Hisatomi, T.; Katayama, M.; Shibata, N.; Yamada, T.; et al. Efficient Hydrogen Evolution on (CuInS<sub>2</sub>)<sub>x</sub>(ZnS)<sub>1-x</sub> Solid Solution-Based Photocathodes under Simulated Sunlight. *Chem. Commun.* **2019**, *55*, 470–473. [[CrossRef](#)] [[PubMed](#)]
13. Kato, T.; Hakari, Y.; Ikeda, S.; Jia, Q.; Iwase, A.; Kudo, A. Utilization of Metal Sulfide Material of (CuGa)<sub>1-x</sub>Zn<sub>2x</sub>S<sub>2</sub> Solid Solution with Visible Light Response in Photocatalytic and Photoelectrochemical Solar Water Splitting Systems. *J. Phys. Chem. Lett.* **2015**, *6*, 1042–1047. [[CrossRef](#)] [[PubMed](#)]
14. Septina, W.; Gunawan; Ikeda, S.; Harada, T.; Higashi, M.; Abe, R.; Matsumura, M. Photosplitting of Water from Wide-Gap Cu(In,Ga)S<sub>2</sub> Thin Films Modified with a CdS Layer and Pt Nanoparticles for a High-Onset-Potential Photocathode. *J. Phys. Chem. C* **2015**, *119*, 8576–8583. [[CrossRef](#)]
15. Guijarro, N.; Prévot, M.S.; Yu, X.; Jeanbourquin, X.A.; Bornoz, P.; Bourée, W.; Johnson, M.; Le Formal, F.; Sivula, K. A Bottom-up Approach toward All-Solution-Processed High-Efficiency Cu(In,Ga)S<sub>2</sub> Photocathodes for Solar Water Splitting. *Adv. Energy Mater.* **2016**, *6*, 1501949–1501961. [[CrossRef](#)]
16. Yokoyama, D.; Minegishi, T.; Maeda, K.; Katayama, M.; Kubota, J.; Yamada, A.; Konagai, M.; Domen, K. Photoelectrochemical Water Splitting Using a Cu(In,Ga)Se<sub>2</sub> Thin Film. *Electrochem. Commun.* **2010**, *12*, 851–853. [[CrossRef](#)]
17. Moriya, M.; Minegishi, T.; Kumagai, H.; Katayama, M.; Kubota, J.; Domen, K. Stable Hydrogen Evolution from CdS-Modified CuGaSe<sub>2</sub> Photoelectrode under Visible-Light Irradiation. *J. Am. Chem. Soc.* **2013**, *135*, 3733–3735. [[CrossRef](#)]
18. Septina, W.; Ikeda, S.; Harada, T.; Minegishi, T.; Domen, K.; Matsumura, M. Platinum and Indium Sulfide-Modified CuInS<sub>2</sub> as Efficient Photocathodes for Photoelectrochemical Water Splitting. *Chem. Commun.* **2014**, *50*, 8941–8943.
19. Septina, W.; Harada, T.; Nose, Y.; Ikeda, S. Investigation of the Electric Structures of Heterointerfaces in Pt- and In<sub>2</sub>S<sub>3</sub>-Modified CuInS<sub>2</sub> Photocathodes Used for Sunlight-Induced Hydrogen Evolution. *ACS Appl. Mater. Interfaces* **2015**, *7*, 16086–16092.
20. Chae, S.Y.; Park, S.J.; Han, S.G.; Jung, H.; Kim, C.W.; Jeong, C.; Joo, O.S.; Min, B.K.; Hwang, Y.J. Enhanced Photocurrents with ZnS Passivated Cu(In,Ga)(Se,S)<sub>2</sub> Photocathodes Synthesized Using a Nonvacuum Process for Solar Water Splitting. *J. Am. Chem. Soc.* **2016**, *138*, 15673–15681. [[CrossRef](#)]
21. Yang, J.; Wang, D.; Han, H.; Li, C. Roles of Cocatalysts in Photocatalysis and Photoelectrocatalysis. *Acc. Chem. Res.* **2013**, *46*, 1900–1909. [[CrossRef](#)] [[PubMed](#)]
22. Yu, X.; Shavel, A.; An, X.; Luo, Z.; Ibáñez, M.; Cabot, A. Cu<sub>2</sub>ZnSnS<sub>4</sub>-Pt and Cu<sub>2</sub>ZnSnS<sub>4</sub>-Au Heterostructured Nanoparticles for Photocatalytic Water Splitting and Pollutant Degradation. *J. Am. Chem. Soc.* **2014**, *136*, 9236–9239. [[CrossRef](#)] [[PubMed](#)]
23. Wang, X.; Ruan, Y.; Feng, S.; Chen, S.; Su, K. Ag Clusters Anchored Conducting Polyaniline as Highly Efficient Cocatalyst for Cu<sub>2</sub>ZnSnS<sub>4</sub> Nanocrystals toward Enhanced Photocatalytic Hydrogen Generation. *ACS Sustain. Chem. Eng.* **2018**, *6*, 11424–11432. [[CrossRef](#)]

24. Osaki, J.; Yoda, M.; Takashima, T.; Irie, H. Selective Loading of Platinum or Silver Cocatalyst onto a Hydrogen-Evolution Photocatalyst in a Silver-Mediated All Solid-State Z-Scheme System for Enhanced Overall Water Splitting. *RSC Adv.* **2019**, *9*, 41913–41917. [[CrossRef](#)]
25. Suzuki, T.M.; Saeki, S.; Sekizawa, K.; Kitazumi, K.; Takahashi, N.; Morikawa, T. Photoelectrochemical Hydrogen Production by Water Splitting over Dual-Functionally Modified Oxide: P-Type N-Doped Ta<sub>2</sub>O<sub>5</sub> Photocathode Active under Visible Light Irradiation. *Appl. Catal. B* **2017**, *202*, 597–604. [[CrossRef](#)]
26. Li, Y.; Luo, K. Performance Improvement of p-Cu<sub>2</sub>O Nanocrystal Photocathode with Ultra-Thin Silver Protective Layer. *Chem. Commun.* **2019**, *55*, 9963–9966. [[CrossRef](#)]
27. Paracchino, A.; Laporte, V.; Sivula, K.; Grätzel, M.; Thimsen, E. Highly Active Oxide Photocathode for Photoelectrochemical Water Reduction. *Nat. Mater.* **2011**, *10*, 456–461. [[CrossRef](#)]
28. Zhao, J.; Minegishi, T.; Zhang, L.; Zhong, M.; Nakabayashi, M.; Ma, G.; Hisatomi, T.; Katayama, M.; Ikeda, S.; Shibata, N.; et al. Enhancement of Solar Hydrogen Evolution from Water by Surface Modification with CdS and TiO<sub>2</sub> on Porous CuInS<sub>2</sub> Photocathodes Prepared by an Electrodeposition—Sulfurization Method. *Angew. Chem. Int. Ed.* **2014**, *53*, 11808–11812. [[CrossRef](#)]
29. Mali, M.G.; Yoon, H.; Joshi, B.N.; Park, H.; Al-Deyab, S.S.; Lim, D.C.; Ahn, S.; Nervi, C.; Yoon, S.S. Enhanced Photoelectrochemical Solar Water Splitting Using a Platinum-Decorated CIGS/CdS/ZnO Photocathode. *ACS Appl. Mater. Interfaces* **2015**, *7*, 21619–21625. [[CrossRef](#)]
30. Koo, B.; Nam, S.W.; Haight, R.; Kim, S.; Oh, S.; Cho, M.; Oh, J.; Lee, J.Y.; Ahn, B.T.; Shin, B. Tailoring Photoelectrochemical Performance and Stability of Cu(In,Ga)Se<sub>2</sub> Photocathode via TiO<sub>2</sub>-Coupled Buffer Layers. *ACS Appl. Mater. Interfaces* **2017**, *9*, 5279–5287. [[CrossRef](#)]
31. Lee, S.M.; Ikeda, S.; Otsuka, Y.; Septina, W.; Harada, T.; Matsumura, M. Homogeneous Electrochemical Deposition of In on a Cu-Covered Mo Substrate for Fabrication of Efficient Solar Cells with a CuInS<sub>2</sub> Photoabsorber. *Electrochim. Acta* **2012**, *79*, 189–196. [[CrossRef](#)]
32. Matoba, K.; Matsuda, Y.; Takahashi, M.; Sakata, Y.; Zhang, J.; Higashimoto, S. Fabrication of Pt/In<sub>2</sub>S<sub>3</sub>/CuInS<sub>2</sub> Thin Film as Stable Photoelectrode for Water Splitting under Solar Light Irradiation. *Catal. Today* **2020**. [[CrossRef](#)]
33. Takashima, T.; Sano, T.; Irie, H. Cocatalyst Modification of Niobium-Substituted Silver Tantalate Photocatalyst for Enhanced Solar Water-Splitting Activity. *Int. J. Hydrogen Energy* **2019**, *44*, 23600–23609. [[CrossRef](#)]
34. Takashima, T.; Sano, T.; Irie, H. Improvement of The Photocatalytic Water Splitting Activity of Silver Tantalate by Photodeposited Platinum and Cobalt-Oxide Nanoclusters. *Electrochemistry* **2016**, *84*, 784–788. [[CrossRef](#)]
35. Kaneko, H.; Minegishi, T.; Higashi, T.; Nakabayashi, M.; Shibata, N.; Domen, K. Stable Hydrogen Production from Water on an NIR-Responsive Photocathode under Harsh Conditions. *Small* **2018**, *2*, 1800018. [[CrossRef](#)]
36. Zhu, W.; Michalsky, R.; Metin, Ö.; Lv, H.; Guo, S.; Wright, C.J.; Sun, X.; Peterson, A.A.; Sun, S. Monodisperse Au Nanoparticles for Selective Electrocatalytic Reduction of CO<sub>2</sub> to CO. *J. Am. Chem. Soc.* **2013**, *135*, 16833–16836. [[CrossRef](#)]
37. Gao, J.; Zhu, C.; Zhu, M.; Fu, Y.; Huang, H.; Liu, Y.; Kang, Z. Highly Selective and Efficient Electroreduction of Carbon Dioxide to Carbon Monoxide with Phosphate Silver-Derived Coral-like Silver. *ACS Sustain. Chem. Eng.* **2019**, *7*, 3536–3543. [[CrossRef](#)]
38. Hori, Y. Electrochemical CO<sub>2</sub> reduction on metal electrodes. In *Modern Aspects of Electrochemistry*; Vayenas, C.G., White, R.E., Gamboa-Aldeco, M.E., Eds.; Springer: New York, NY, USA, 2008; Volume 42, pp. 89–189.
39. Ikeda, S.; Fujikawa, S.; Harada, T.; Nguyen, T.H.; Nakanishi, S.; Takayama, T.; Iwase, A.; Kudo, A. Photocathode Characteristics of a Spray-Deposited Cu<sub>2</sub>ZnGeS<sub>4</sub> Thin Film for CO<sub>2</sub> Reduction in a CO<sub>2</sub>-Saturated Aqueous Solution. *ACS Appl. Energy Mater.* **2019**, *2*, 6911–6918. [[CrossRef](#)]
40. Ikeda, S.; Tanaka, Y.; Kawaguchi, T.; Fujikawa, S.; Harada, T.; Takayama, T.; Iwase, A.; Kudo, A. Photoelectrochemical Reduction of CO<sub>2</sub> to CO Using a CuGaS<sub>2</sub> Thin-film Photocathode Prepared by a Spray Pyrolysis Method. *Chem. Lett.* **2018**, *47*, 1424–1427. [[CrossRef](#)]
41. Kamimura, S.; Sasaki, Y.; Kanaya, M.; Tsubota, T.; Ohno, T. Improvement of Selectivity for CO<sub>2</sub> Reduction by Using Cu<sub>2</sub>ZnSnS<sub>4</sub> Electrodes Modified with Different Buffer Layers (CdS and In<sub>2</sub>S<sub>3</sub>) under Visible Light Irradiation. *RSC Adv.* **2016**, *6*, 112594–112601. [[CrossRef](#)]
42. Nesbitt, N.T.; Ma, M.; Trzeźniewski, B.J.; Jaszewski, S.; Tafti, F.; Burns, M.J.; Smith, W.A.; Naughton, M.J. Au Dendrite Electrocatalysts for CO<sub>2</sub> Electrolysis. *J. Phys. Chem. C* **2018**, *122*, 10006–10016. [[CrossRef](#)]

43. Urbain, F.; Tang, P.; Carretero, N.M.; Andreu, T.; Arbiol, J.; Morante, J.R. Tailoring Copper Foam with Silver Dendrite Catalysts for Highly Selective Carbon Dioxide Conversion into Carbon Monoxide. *ACS Appl. Mater. Interfaces* **2018**, *10*, 43650–43660. [[CrossRef](#)] [[PubMed](#)]
44. Kaur, M.; Nagaraja, C.M. Template-Free Synthesis of  $Zn_{1-x}Cd_xS$  Nanocrystals with Tunable Band Structure for Efficient Water Splitting and Reduction of Nitroaromatics in Water. *ACS Sustain. Chem. Eng.* **2017**, *5*, 4293–4303. [[CrossRef](#)]
45. Hernández-Calderón, V.; Vigil-Galán, O.; Pulgarín-Agudelo, F.A.; Courel, M.; Arce-Plaza, A.; Cruz-Gandarilla, F.; Sánchez-Rodríguez, F.J.; Roque-De la Puente, J. Optimization of  $Cd_xZn_{1-x}S$  Compound from CdS/ZnS Bi-Layers Deposited by Chemical Bath Deposition for Thin Film Solar Cells Application. *Thin Solid Films* **2019**, *676*, 100–107. [[CrossRef](#)]



© 2020 by the authors. Licensee MDPI, Basel, Switzerland. This article is an open access article distributed under the terms and conditions of the Creative Commons Attribution (CC BY) license (<http://creativecommons.org/licenses/by/4.0/>).